Published in final edited form as:
Mol Pharm. 2013 June 3; 10(6): 2237–2247. doi:10.1021/mp300613x.

Non-Invasive Monitoring of Pulmonary Fibrosis by Targeting Matrix Metalloproteinases (MMPs)

Yan Cai[1,§], **Lei Zhu**[2,3,§], **Fan Zhang**[3], **Gang Niu**[3], **Seulki Lee**[3], **Shioko Kimura**[1,*], and **Xiaoyuan Chen**[3,*]

[1]Laboratory of Metabolism, National Cancer Institute, National Institutes of Health, Bethesda, MD 20892, USA

[2]Center for Molecular Imaging and Translational Medicine, School of Public Health, Xiamen University, Xiamen, 361005, China

[3]Laboratory of Molecular Imaging and Nanomedicine (LOMIN), National Institute of Biomedical Imaging and Bioengineering, National Institutes of Health, Bethesda, MD 20892, USA

Abstract

While idiopathic pulmonary fibrosis (PF) is a devastating lung disease, the management of PF including effective monitoring of disease progression remains a challenge. Herein, we introduce a novel, fast and ultra-sensitive metalloproteinase (MMP) activatable optical probe, named MMP-P12, to non-invasively monitor PF progression and response to PF treatment. A bleomycin (BLM)-induced mouse PF model was subjected non-invasively to optical imaging at various time points after BLM treatment. Mouse PF model developed fibrosis during 21 days of experimental period, and the progression of PF was well correlated with the step-wise increase of MMP-2 expression as examined by quantitative RT-PCR and western blot analysis on the 7-, 14-and 21-day post-BLM administration. On these days, MMP-activated fluorescence images were acquired *in vivo* and *ex vivo*. Signal quantification showed time-dependent lung-specific incremental increases in fluorescence signals. As a treatment for PF, secretoglobin 3A2 was daily administered intravenously for five days starting day seven of BLM administration, which resulted in reduced MMP-2 activity and reduction of PF as previously demonstrated. Importantly, the fluorescence signal that reflected MMP activity also decreased in intensity. In conclusion, MMPs may play an important role in PF development and MMP-P12 probe could be a promising tool for PF detection, even at an early stage of the disease as well as an indicator of therapy response.

Keywords

Pulmonary fibrosis; Matrix metalloproteinase; Optical imaging; Activatable probe; Secretoglobin 3A2

1. Introduction

The lung is affected by many diseases that may lead to considerable morbidity and mortality,[1] including pulmonary fibrosis (PF), a serious disease in which the lungs become progressively scarred or thickened for unknown reasons.[2] In the healthy body, the

*To whom correspondence should be addressed. Tel: +1 301 451 4246, Fax: +1 301 480 1679; shawn.chen@nih.gov (X.C.) or kimuras@mail.nih.gov (S.K.).
§Y. C. and L. Z. contributed equally to this work.

The authors declare no competing financial interest.

bloodstream carries oxygen from alveoli to all organs. In PF patients, the scarred and thickened alveoli and interstitial area stop oxygen's movement into the bloodstream,[3] causing serious shortness of breath, tiredness, gradual weight loss and other fatal symptoms. The presence of fibrosis in lung could also significantly increase the risk of generating tumor foci.[4, 5] Most people survive only for about three to five years after diagnosis. To date, there are no proven effective therapies available for this disease and lung transplant is the only way currently available to prolong survival of patients in late-stage of PF. Thus, the management of PF remains a challenge.

Although the pathogenic mechanisms of PF are not fully understood,[6] based on the observations from both animal models and patients with PF, it is believed that a family of matrix metalloproteinases (MMPs) play a central role in PF.[7, 8] MMPs are a family of Zn^{2+}-dependent endopeptidases that is involved in the breakdown and remodeling of extracellular matrix (ECM) under a variety of physiological and pathological conditions.[9] Based on their substrates, MMPs can be classified into collagenases, matrilysins, gelatinases and stromelysins.[10] MMP-2, also known as the gelatinase-A, is particularly important in the pathogenesis of inflammatory, infectious, and neoplastic diseases in many organs including the lung. It is secreted as an inactive zymogen (pro-MMP-2), which can be activated to hydrolyze denatured collagen (gelatine), native type IV and V collagens, elastine and certain ECM components.[7, 9, 11] The activation process of MMPs *in vivo* is balanced by the activity of specific tissue inhibitor of matrix metalloproteinases. In encapsulating peritoneal sclerosis patients[12–14] and the bleomycin (BLM)-induced mouse PF model,[15, 16] MMP-2 activity was elevated. Moreover, inhibition of MMP-2 and other MMPs' activity by a pan-MMP inhibitor ameliorated the development of lung fibrosis in the mouse PF model.[17, 18] While the function of MMP-2 has been well studied in the PF model, the application of using MMP-2 as PF diagnosis target has not been reported.

BLM is the most widely used agent, and often regarded as the standard in modeling PF. BLM sulfate is a mixture of cytotoxic glycopeptide antibiotics and is used as an antineoplastic/antibiotic drug to treat various cancers. It acts by causing DNA breaks in tumor cells, subsequently inducing apoptosis.[2] However, repeated systemic administration of BLM may cause lung fibrosis as the main side effect.[19, 20] In the PF model rodents, the most common route of BLM administration is intratracheal, which generally causes an inflammatory response and increased epithelial apoptosis in lung within the first seven days with a pathophysiology closely resembling acute lung injury. This is followed by three days of transitional period, where inflammation resolves and fibrosis is detected. The fibrotic stage persists until three to four weeks post-BLM, characterized by excessive deposition of ECM, causing areas of fibrosis.[3]

Fluorogenic substrates, consisting of protease substrates labeled with a fluorescent reporter and a quencher dye, are highly sensitive and sequence specific, and have long been used in *in vitro* diagnostic assays.[21] Recent advances in optical imaging instrument and development of various near-infrared (NIR) fluorescent dyes and NIR quenchers enabled the use of conventional fluorogenic substrates for *in vivo* imaging applications.[22–27] We have previously reported optimization of a MMP activatable probe *in vivo*.[28] A series of modified MMP probes conjugated with various sizes of polyethylene glycol (PEG) were screened in tumor-bearing mice. We found that the MMP probe conjugated with PEG12 (MMP-P12) showed the fastest enzyme recognition and degradation properties among the probes examined. In view of the important roles of MMPs, especially MMP-2, in PF, we herein applied the ultra-fast MMP sensor, MMP-P12, in a BLM-induced mouse lung fibrosis model for diagnosis and monitoring PF treatment response. By optical imaging of PF mediated by MMP-P12, we successfully assessed the severity of PF and the response to the treatment of PF. The PF can be detected at early stage (seven days post-BLM inducement) and the

treatment effect was verified by MMP-P12-mediated optical imaging, suggesting that MMP-P12 might be a promising tool for PF assessment.

2. Materials and Methods

2.1. Chemicals

Cy5.5 N-hydroxy succinimide (NHS) ester was purchased from GE Healthcare (Piscataway, NJ). Black hole quencher-3 (BHQ-3) was from Bioresearch technologies (Novato, CA). The amino acids and peptide synthesis related reagents were obtained from CS Bio. Co. (Menlo Park, CA). TRIzol and Superscript II reverse transcriptase were purchased from Invitrogen Corporation (Carlsbad, CA). Rabbit anti-MMP-2 antibody was bought from Abcam (Cambridge, MA). β-actin primary antibody was bought from Santa Cruz Biotechnology, Inc (Santa Cruz, CA). Recombinant mouse SCGB3A2 was prepared as previously described.[29] All other solvents and reagents were purchased from Sigma-Aldrich (St. Louis, MO).

2.2. Animals and SCGB3A2 Treatment

C57BL/6N mice (NCI Frederick, National Institutes of Health) were maintained under a standard 12-h light/12-h dark cycle with water and chow provided ad libitum. At least ten 7–8-week-old C57BL/6N mice were used for each group. BLM (1.5 units/kg, Sigma) or PBS as control was directly administered once by intratracheal intubation using the BioLITE system (BioTex, Inc., Houston, TX). Purified recombinant mouse SCGB3A2 (0.25 mg/kg/day) or PBS was intravenously administered to mice via the tail vein once daily for five days starting on the 7th day after BLM administration. Three groups of mice were used in this study; administration of BLM followed by intravenous injection of PBS or SCGB3A2 or administration of PBS followed by intravenous injection of PBS. Mice were euthanized on day 21, and bronchoalveolar lavage (BAL) fluids were obtained by lavaging lungs with 1 mL PBS. The collected BAL fluids were used for counting inflammatory cell numbers. All animal studies including imaging studies were performed after approval by the National Cancer Institute and National Institute of Biomedical Imaging and Bioengineering Animal Care and Use Committees.

2.3. Quantitative RT-PCR

Total RNAs isolated using TRIzol and digested with DNase I were reverse-transcribed by Superscript II reverse transcriptase. Quantitative RT-PCR was performed with ABI Prism 7900 Sequence Detection System (Applied Biosystems, Foster City, CA) using SYBR Green master mixture. The ΔΔCt method was used using β-actin as normalization control. PCR condition used was 50 °C, 2 min and 95 °C, 10 min followed by 95 °C, 15 sec and 60 °C, 40 sec for 40 cycles with the following primers:

Mmp2 forward: GGG GTC CAT TTT CTT CTT CA

Mmp2 reverse: CCA GCA AGT AGA TGC TGC CT

β-actin forward: ATG GAG GGG AAT ACA GCC C

β-actin reverse: TTC TTT GCA GCT CCT TCG TT

2.4. Western blot analysis

Minced lung tissues were washed in PBS and lysed in radio-immuno-protein-assay buffer (20 mM Tris-HCl, 150 mM NaCl, 0.1% SDS, 0.1% sodium deoxycholate, 1% Triton X-100, 2 mM EDTA, 10 mM sodium fluoride, and 1 mM sodium orthovanadate) with Protease Inhibitor Cocktail Tablets (Complete Mini; Roche). The lysates were mixed with SDS sample loading buffer containing 2-mercaptoethanol, electrophoresed on 10% SDS-

polyacrylamide gels containing 0.1 or 0.8% bis-(N,N″-methylene-bis-acrylamide), and then electrotransferred to an Immobilon-P membrane (Millipore). Membranes were blocked with TBS-Tween (20 mM Tris-HCl, pH 7.5, 150 mM NaCl, and 0.1% Tween 20) and 5% skin milk, and were incubated with the following primary antibody in TBS-Tween; MMP-2, SM22 α-actin, and β-actin. Membranes were washed with TBS-Tween, and then incubated with HRP-conjugated secondary antibody (Santa Cruz Biotechnology). Protein bands were detected using Western Lightning Chemiluminescence Reagent Plus (PerkinElmer), followed by exposure to scientific imaging film (Eastman Kodak) or quantitation with FluoChem HD2 (Alpha Innotech, Santa Clara, CA).

2.5. Pathology

The whole lung was inflated and fixed with 4% paraformaldehyde. Lung tissues were embedded in paraffin, and 4-μm whole lung sections were prepared. Hematoxylin and eosin staining was carried out for assessment of BLM-induced fibrosis. Masson's trichrome staining was used to detect collagen fibers.

2.6. Quantitation of hydroxyproline content in the lung

Hydroxyproline content was measured using hydroxyproline assay kit from Biovision (Milpitas, CA) according to the manufacture's instruction with slight modification. In brief, whole lungs were homogenized in dH_2O, using 100 μL H_2O for every 10 mg of tissue. To a 100 μL sample of homogenate, 200 μL concentrated HCl (6 N) was added in a pressure-tight, teflon capped vial, and the mixture was hydrolyzed at 120 °C for 3 h, followed by filtration through a 45-μm syringe filter (Millipore, Bedford, MA). 10 μl of each hydrolyzed sample was transferred to a 96-well plate and was evaporated to dryness under vacuum. 100 μL of Chloramine T reagent was added to each sample and standard, and were incubated at room temperature for 5 min. DMAB reagent (100 μL) was then added to each well and further incubated for 90 minutes at 60°C. Absorbance was measured at 560 nm in a microplate reader (SpectroMax Plus384, Molecular Devices, Sunnyvale, CA).

2.7. In vivo optical imaging

The MMP-P12 probe (100 μL in PBS pH 7.4) was intravenously injected via the tail vein 2 hours before imaging. Hair from the chest was removed by shaving and chemical depilation before mice were scanned to avoid autofluorescence signals. Optical imaging was performed using Maestro 2.0 imaging system (CRI, Woburn, MA, USA) configured for Cy5.5 detection (Cy5.5: excitation = 675 nm, emission = 695 nm). During injection and image acquiring process, mice were anesthetized with 2.5% isoflurane in oxygen at a flow of 1.5 L/min. Images were normalized to the same scale and analyzed by using Maestro 2.0 software. For semi-quantitative comparison, the regions of interest (ROI) were drawn over the tissues of interest, and the scaled average signal (photons×cm^{-2}×s^{-1}) for each area was measured. Fluorescent signals from ROI were further corrected by the mice body weights. Results were presented as the mean ± SD for a group of 5 animals.

2.8. Ex vivo biodistribution

Ex vivo imaging of excised lung and other organs gave further confirmation of the targeting specificity of MMP-P12. Mice model with PF were injected with MMP-P12 to evaluate the distribution of MMP2 activatable probe in the lung and the major organs. At 2 hours post injection, the PF mice were sacrificed and their major organs and tissues were carefully harvested and rinsed with saline, and placed on black paper for *ex vivo* imaging. For quantitative comparison, the regions of interest (ROIs) were drawn over the tissues of interest, and the scaled average signal (photons×cm^{-2}×s^{-1}) for each area was measured. Results were presented as the mean ± SD for a group of 5 animals.

2.9. Immunohistochemical staining

Lungs were collected from PF mice to make frozen tissue blocks. These lung specimens were subsequently sectioned in a thickness of 10 μm. Slides were dried in the air and fixed with cold acetone for 20 min and dried again in the air for 30 min at room temperature. After blocking with 10% BSA for 30 min, the sections were incubated with rabbit anti-MMP2 antibody (10 μg/mL) for 60 min at room temperature in the dark, and then treated with Cy3-conjugated donkey anti-rabbit secondary antibody. Finally, the slices were mounted with DAPI-containing mounting medium. To visualize the MMP-P12 signal, the lung slices were directly observed under an epifluorescence microscope (Olympus, X81). Red color is from Cy3 for MMP2 expression visualization and green color is from Cy5.5 for cleaved MMP-P12 distribution. Blue color is from DAPI for nuclei visualization. Original magnification was ×400.

2.10. Statistical Methods

Results were presented as the mean ± SD. Statistical analysis was performed using one-way ANOVA followed by Bonferroni multiple comparison test. $P<0.05$ was considered as statistically significant.

3. Results

3.1. Correlation between the development of PF and increased MMP expression

Fibrosis is among disorders where MMPs are known to play a role.[12, 16] The involvement of MMP2 in the development of PF was demonstrated in the BLM-induced PF model, in which mice were intratracheally intubated with BLM or PBS as control on day 0. The body weights were monitored during 21 days of entire experimental period. Compared with PBS group, the body weight of mice received BLM continuously decreased down to 80% of the original weight (Fig. 1A). Lungs taken from control and the experimental BLM groups on day 7, 14 and 21 after H&E staining demonstrated that mice administered BLM exhibited significantly increased inflammation and fibrosis as post-BLM days increased (Fig. 1B). Histological analysis of lung sections revealed significantly increased inflammation in the first week of BLM administration, which is consistent with the previous report.[30] Masson's trichrome staining of lung sections prepared from day 21 mice demonstrated that the collagen expression in lungs of BLM-administered group was clearly detected in the thickened interstitial space whereas very little collagen expression was found in PBS-administered group (Fig. 1B, right).[29, 31] The levels of *Mmp2* mRNA increased by 4.25±0.84, 6±1.05, and 9±1.87 folds, respectively on day 7, 14, and 21 days post-BLM administration, as compared with PBS-treated control lungs as determined by qRT-PCR (Fig. 1C). The levels of activated MMP2 protein were determined at different stages of PF lungs by western blot analysis (Fig. 1D). The MMP-2 protein levels gradually increased and reached to peak at 21 days, while the level of α-smooth muscle actin drastically increased toward the end of experimental period. These results confirmed that MMP-2 expression was correlated with development of BLM-induced lung fibrosis.

3.2. In vivo detection of MMP activity correlating with PF severity

We previously demonstrated that MMP-P12 could be effectively degraded by MMP-2 in a tumor-bearing mouse model.[28] This was supported by the modeling analysis, showing the high affinity of MMP-P12 to MMP-2 (see the Materials and Methods, Fig. S1–S3, Table S1 and S2 in the online supplement). MMP-P12 remained in a quenched status until being degraded by MMP-2 *in vitro* and/or *in vivo*, which resulted in intense fluorescent signals.

In order to determine whether the MMP-P12 probe could be used for detecting PF in a BLM-induced mouse model, mice were subjected to non-invasive optical imaging after 7,

14, and 21 days of BLM administration (Fig. 2A). Before imaging, the same amount of MMP-P12 was intravenously injected into each mouse, and allowed for two hours to have MMP-P12 thoroughly circulate *in vivo*. Two hour time point was chosen because MMP-P12 probe was found to be stable in healthy mouse blood for this amount of time (Fig. S4). For semi-quantitative comparison, the regions of interest (ROI) were drawn over the tissues of interest, and the scaled average signal (photons×cm^{-2}×s^{-1}) for each area was measured. Fluorescent signals from ROI were further corrected by the mice body weights. The fluorescence imaging signal from the area where lung was located gradually increased over 21 days of experimental period (Fig. 2B). To compare the fluorescence intensity, a region of interest (ROI) was arbitrarily chosen and the intensity was quantified (Fig. 2C). The fluorescence signal increased by 3.86±0.36, 7.11±1.21, and 12.99±0.70 fold on day 7, 14, and 21 days in post-BLM lungs, respectively, as compared with PBS-injected control lungs (Fig. 2D). In accordance with the results described in Fig. 1, the fluorescence signal was correlated with the development of PF and an increscent in the presence of active MMP-2. These data demonstrated that a positive correlation between MMP-2 and PF severity can be non-invasively detected by fluorescence-based optical imaging. The fluorescent signal intensity in ROI and a total number of inflammatory cells present in bronchoalveiolar lavage fluids demonstrated a positive correlation

To confirm the *in vivo* observations, we further evaluated the fluorescent signal recovery of MMP-P12 in the PF model *ex vivo*, using major organs carefully extracted from mice that had undergone a non-invasive optical imaging. A strong signal was found in the lung, and the signal increased accordingly with PF development (Fig. 3A). In addition, the liver and kidney also showed fairly strong fluorescence signals, which were in agreement with the previous observations in tumor imaging experiments,[28] suggesting a potential *in vivo* MMP-P12 metabolism pathway in these organs. Lung was basically the only organ with progressive increase of fluorescent signals in a time-dependent fashion, having >7-fold increase on day 21 as compared with the control group (Fig. 3B). The other organs virtually had unaltered fluorescent intensity during the entire 21 days. These *ex vivo* analysis confirmed the *in vivo* results, demonstrating that MMP-2 activity as the fluorescent signal readout correlated with the development of PF.

In order to verify that the increase of fluorescent signal observed *in vivo* and *ex vivo* as described above was not due to the accumulation of non-specific cleavage of MMP-P12 probe that may have occurred by secretory MMPs present in circulation, a fragment containing a portion of the cleaved MMP-P12 with Cy5.5 conjugated, was synthesized as a control probe (tentatively named as Met) (Fig. S7). Met was used to determine whether fluorescence signal accumulates in PF lungs (Fig. S8 and S9). The results demonstrated that the control probe had very little accumulation in organs examined including day 21 lungs of PF model mice. The accumulation was observed only when PF model mice were injected with MMP-P12 probe.

Thus, MMP-2 may serve as a target for diagnosis and assessment of the severity of PF and that MMP-P12 can be a surrogate for monitoring PF *in vivo*.

3.3. In vivo assessment of PF therapy response

Given the fact that the increase of active MMP-2 protein is correlated with PF development, we next studied whether treatment of PF would decrease the level of active MMP2 protein. To this end, secretoglobin (SCGB) 3A2 was administered to treat the BLM-induced PF model. We previously demonstrated that SCGB3A2 possesses anti-inflammatory, growth factor, and anti-fibrotic activities, and SCGB3A2 was successfully used to suppress/reduce BLM-induced PF in mouse model.[29, 32, 33] BLM-intubated mice were given SCGB3A2 protein intravenously on day 7 of BLM treatment and daily thereafter for a total of five days

as a therapy for PF (see Fig. 5A). Mice that received BLM significantly lost their body weight (~20%) by day 21, while BLM-intubated and SCGB3A2-treated group of mice lost weight only by approximately 10% (Fig. 4A). Masson's Trichrome staining of lung sections prepared from day 21 mice demonstrated that the collagen expression in lungs of SCGB3A2-administered group was much lower than that of BLM only-treated group, where high collagen expression was found as previously reported [29] (Fig. 4B). The qRT-PCR and western blot confirmed that *Mmp2* mRNA and active MMP-2 protein expression were indeed decreased in SCGB3A2-treated group as compared with no treatment group (Fig. 4C, 4D and Fig. S5), demonstrating that MMP2 may serve as a potential target for monitoring PF development.

When these mice were subjected to optical imaging analyses with the MMP-P12 probe, the fluorescence signal in PF mice without SCGB3A2 treatment was 10.92±2.06 times higher than normal mice, while only a 4.82±0.87 times higher fluorescent signal was collected in the PF model treated with SCGB3A2 (Fig. 5B and 5C). The decreased florescent signal in SCGB3A2-treated fibrotic lungs agreed with their lower expression of *Mmp2* mRNA and active MMP-2 protein as shown in Fig. 4, again clearly demonstrating that MMP-P12 fluorescent signal was positively correlated with the MMP2 expression in PF model *in vivo*. The relationship between MMP-2 expression and PF was further confirmed by *ex vivo* imaging analysis of BLM PF model and SCGB3A2-treated lungs (Fig. 5D and 5E). Taken together, these results demonstrated that MMP-P12 is capable of detecting MMP-2 in the PF model, non-invasively monitoring PF therapy response, and possibly staging PF.

3.4. Fluorescent signal recovery of MMP-P12 in lung sections

In order to confirm that the fluorescent signal indeed came from MMP-2-mediated MMP-P12 fluorescent signal recovery, lung sections were prepared from fibrotic lungs for MMP-2 immunofluorescence (Fig. 6, red color) and the direct fluorescence signal derived from MMP-P12 cleavage (green color). A strong fluorescent signal due to MMP-P12 cleavage was found in fibrotic lungs while a weak signal was seen in normal lung sections, which agreed with more MMP-2 expression in the fibrotic lung than normal lung. The MMP-P12 cleavage signals overlapped with MMP-2 expression as seen in yellow color (see Merge image). Both green and red signals were weak in SCGB3A2-treated lung sections, suggesting that the expression of MMP-2 was reduced, which was reflective of reduced development of PF by SCGB3A2 treatment.

4. Discussion

We reported herein the application of an optical activatable probe for non-invasive diagnosis of PF and monitoring of its response to therapy in the BLM-induced mouse model by targeting MMP-2. We firstly confirmed that MMP-2 expression was correlated with PF development by histology, qRT-PCR and western blot. The fluorescent signal detected from fibrotic lungs due to cleavage of the activatable probe MMP-P12 was positively correlated with the expression of MMP-2 at different stages of PF (7, 14 and 21 days after BLM administration). Notably, liver was found to have an increased fluorescence signals over time. One of the possible reasons is that more MMPs are secreted into the blood stream with the development of PF and in turn causing more MMP-P12 cleavage. The Cy5.5 containing portion of the cleaved MMP-P12 accumulates in the liver and shows an increased optical signal. However, a Met fragment having the same Cy5.5 containing portion of the cleaved MMP-P12 as positive control did not increase fluorescence signals over time beyond background, further supporting our conclusion that MMP-P12 derived signal was correlated with the expression of MMP-2 in PF model (Fig. S7, Fig. S8, and Fig. S9). When fibrosis development was reduced after SCGB3A2 treatment, the fluorescent signal was decreased due to the reduced expression of MMP-2. Taken together, these results revealed that our

approach is proven to be a fast and sensitive method to detect MMP-2 activity *in vivo* even at early stages of PF development such as 7 days after BLM inducement, which is associated with the severity of PF. In addition, the probe MMP-P12 demonstrated its potential in monitoring the PF therapy response in mouse model. SCGB3A2 and MMP-P12 imaging may indeed be a good combinatorial tool to monitor and/or treat PF.

Early diagnosis and monitoring of the therapeutic response of PF are important for preclinical and clinical investigation of PF. However, accurate diagnosis of PF is challenging since many lung diseases exhibit similar symptoms. Currently, the diagnosis of PF has moved from traditional invasive histological studies to less invasive methods such as continuous testing of patients' lung functions. With the development of molecular imaging techniques, non-invasive imaging has been recently applied in clinical diagnosis of PF. For example, high resolution computed tomography (HRCT) is the current imaging reference standard in the investigation of patients with PF.[3] HRCT is capable of revealing structural details of the entire lung and monitoring the response to PF treatment.[34] However, HRCT is a structural imaging modality which only provides indirect metabolism inferences.[3] Another imaging modality for diagnosis of PF is positron emission tomography (PET) imaging. In recent years, ^{18}F-fluorodeoxyglucose (^{18}F-FDG) PET has emerged as a reliable diagnosis method with decent sensitivity.[35, 36] However, ^{18}F-FDG PET has some pitfalls when distinguishing lung inflammation from lung fibrosis.[37] Furthermore, no studies have demonstrated the parallel relationship between ^{18}F-FDG uptake and PF patient's survival.[3] Pertechnegas and ^{99m}Tc diethylenetriamine pentacetate can be applied for measuring the alveolar capillary membrane permeability in the lung, but the accuracy of this method is low.[3] For nuclear imaging, there will be high cost of instruments, labor and a special way of dealing with the nuclear waste, and more importantly, a repeated application to the patients is limited. Therefore, more work is needed in developing new molecular imaging agents that is less expensive with higher safety than nuclear imaging but also could provide specific and direct information of fibrosis for early diagnosis and assessment of treatment response.

Enzyme activity-based activatable probes have been successfully applied to visualize *in vivo* expression of proteases, along with the development of optical imaging.[38, 39] It holds advantages over other imaging agents in terms of no radiation, low background and high target specific recognition properties. By our *in vitro* and *in vivo* experiments, a positive correlation between MMP-2 expression and PF development was found. Some other groups also reported that MMP-2 was found to be closely correlated to lung disease and could be a target for imaging allergic airway inflammation.[12] Cortez-Retamozo *et al.* reported the utilization of a pan-MMP optical sensor, MMPSense-680, for the diagnosis of allergic airway inflammation and the assessment for the response to treatment.[40] The inflammation and recovery of lung inflammation were successfully visualized 24 hours after injection of MMPSense-680 by FMT and NIRF bronchoscopy. However, the detection of PF by activatable probe has not been investigated. In our previous study, different lengths of PEG were conjugated MMP-2 substrate peptide beacon.[28] The effect of PEG length was considered to affect the enzyme degradation efficiency to MMP-PEG analogs and also the half-life of the probe. As we mentioned before, we found MMP-P12 demonstrated the best MMPs detection efficiency in tumor model. Herein, the MMP-P12 probe we applied demonstrated a faster recovery of fluorescent signal (2 hours post injection) and was potential to monitor the PF therapy response that can be repeated. These results suggested that the small peptide probe would be of much more benefit for probing the development and treatment of PF.

The human genome encodes roughly two dozen MMPs.[9] For many MMP members, their substrate specificity is relatively broad and probably overlapping. Therefore, it is a challenge to develop a specific MMP substrate or MMP inhibitors (MMPIs). A broad spectrum

MMPIs may not only suppress the MMP in disease area but will also decrease the MMP activity that plays a role in physiological condition. This will induce many other fatal side effects, which was and still is hampering application of MMPIs into clinic for certain diseases therapy.[41, 42] However, the specificity of targeting MMPs for diagnosis purpose is not as critical as therapeutic inhibitors. In most cases more than one MMP is involved in the disease; for example, in tumor development MMP-2, MMP-9, and MMP-14 play major roles, while during rheumatoid arthritis development, MMP-2 and MMP-13 are considered as the key players.[43] A probe that targets certain MMPs would be of benefit to improve the detection efficiency where multiple MMPs are involved. The MMP-P12 can be degraded by MMP-2, MMP-9 and MMP-13, but poorly cleaved by MMP-3 and MMP-7 as previously reported.[28] In our study, we mainly studied the gene expression and active MMP-2 expression relationships with development of PF. With the development of PF, MMP-2 gene and protein expressions were found to be obviously elevated. We also noticed that other MMPs may also play a role in PF development, but herein MMP-2 was chosen as a representative for the MMPs members. A bioluminescence and optical dual imaging system may be helpful to better understand the probe distribution in vivo.[44] However, due to the specific limitation of the probe, the optical signal we detected here was likely to be generated by a number of MMPs and reflecting the overall MMP expression. There is currently no better way to tell the direct links between individual MMP to PF. Since the affinity of MMP-2:MMP-P12 complex seemed to be quite high as determined by modeling analysis (see the online supplement), in view of the role of MMPs in PF development,[12, 17, 45] we chose MMP-2 as our target for diagnosis and monitoring of therapy response in PF mouse model. A positive correlation was found between MMP-2 expression and PF development.

It is possible that with the development of PF, increasing MMP-2 was secreted and its concentration in blood was elevated, which may have caused some non-specific fluorescence signal recovery in tissues other than lung (Fig. 2, 3 and 5). However, only lung demonstrated a drastic increase in fluorescent signal ($p < 0.05$) as PF progressed. To address these concerns, MMP-P12 stability was first studied in both healthy and PF mouse blood (Fig. S4). MMP-P12 was found stable in healthy mouse blood for two hours after injection, while it was observed degraded in PF mouse blood after approximately 15 minutes. This may be due to the elevated levels of secreted MMPs in circulation of PF mouse, which quickly degraded MMP-P12. Moreover, to determine if non-specific cleavage fragment has contributed fluorescent signals, we synthesized a fragment and conjugated with NIR dye Cy5.5, which we tentatively named as Met (Fig. S7). This fragment was the one cleaved by MMP between Gly and Val in the probe as reported by us and other researchers. After injection of Met into PBS and PF mouse model, we did not observe obvious Met accumulation in neither normal nor PF lungs compared with that of MMP-P12 administrated PF model (Fig. S8). *Ex vivo* data also confirmed very little lung accumulation of Met (Fig. S9). By using this stable and sensitive MMP activatable probe, we provide an efficient approach for diagnosis and monitoring therapy response of PF. In the view of that BLM pulmonary toxicity is a severe complication of BLM treatment and there is no good way to monitor the development of BLM toxicity at present in the clinic, the MMP-2:MMP-P12 imaging protocol may be used as the reporter for a measure of BLM toxicity, in particular as a means to monitor toxicity before it becomes clinically apparent.

5. Conclusion

In summary, our results demonstrated that the progression of PF can be detected using a MMP activatable optical probe, MMP-P12, in conjunction with a whole body non-invasive fluorescence imaging technology in mice. Since MMPs including MMP-2 are known to be increased in tumors, this technology may be successfully applied to the detection of tumor

progression. Thus, MMP-2 would serve as a potential biomarker for early diagnosis of lung fibrosis and tumor, and will lead to a new dimension in discovering therapeutic tools for the prevention and/or treatment of these diseases.

Supplementary Material

Refer to Web version on PubMed Central for supplementary material.

Acknowledgments

This work was supported by the Major State Basic Research Development Program of China (973 Program) (No. 2013CB733802), National Science Foundation of China (NSFC) (81201129, 81101101, 81201086, 81201190, and 51273165), Chinese Academy of Sciences professorship for Senior International Scientists (2011T2J06), Key Project of Chinese Ministry of Education (212149), and the Intramural Research Program (IRP) of the National Institute of Biomedical Imaging and Bioengineering (NIBIB) and the National Cancer Institute (NCI), National Institutes of Health (NIH). We thank Frank Gonzalez for his critical review of the manuscript. We also thank Jerrold M. Ward (Global VetPathology, Montgomery Village, Maryland) for histological analysis in this manuscript.

References

1. Martinez FJ, Donohue JF, Rennard SI. The future of chronic obstructive pulmonary disease treatment--difficulties of and barriers to drug development. Lancet. 9795; 378:1027–37. [PubMed: 21907866]
2. American Thoracic Society. Idiopathic pulmonary fibrosis: diagnosis and treatment. International consensus statement. American Thoracic Society (ATS) and the European Respiratory Society (ERS). Am J Respir Crit Care Med. 2000; 161(2 Pt 1):646–64. [PubMed: 10673212]
3. Thomeer M, Grutters JC, Wuyts WA, Willems S, Demedts MG. Clinical use of biomarkers of survival in pulmonary fibrosis. Respir Res. 2010; 11:89. [PubMed: 20584284]
4. Lee HJ, Im JG, Ahn JM, Yeon KM. Lung cancer in patients with idiopathic pulmonary fibrosis: CT findings. J Comput Assist Tomogr. 1996; 20(6):979–82. [PubMed: 8933802]
5. Artinian V, Kvale PA. Cancer and interstitial lung disease. Curr Opin Pulm Med. 2004; 10(5):425–34. [PubMed: 15316443]
6. Selman M, King TE, Pardo A. Idiopathic pulmonary fibrosis: prevailing and evolving hypotheses about its pathogenesis and implications for therapy. Ann Intern Med. 2001; 134(2):136–51. [PubMed: 11177318]
7. Dancer RC, Wood AM, Thickett DR. Metalloproteinases in idiopathic pulmonary fibrosis. Eur Respir J. 2011; 38(6):1461–7. [PubMed: 21700608]
8. Suga M, Iyonaga K, Okamoto T, Gushima Y, Miyakawa H, Akaike T, Ando M. Characteristic elevation of matrix metalloproteinase activity in idiopathic interstitial pneumonias. Am J Respir Crit Care Med. 2000; 162(5):1949–56. [PubMed: 11069839]
9. Kessenbrock K, Plaks V, Werb Z. Matrix metalloproteinases: regulators of the tumor microenvironment. Cell. 2010; 141(1):52–67. [PubMed: 20371345]
10. Zhu L, Wang H, Wang L, Wang Y, Jiang K, Li C, Ma Q, Gao S, Li W, Cai M, Niu G, Lee S, Yang W, Fang X, Chen X. High-affinity peptide against MT1-MMP for in vivo tumor imaging. J Control Release. 2011; 150(3):248–55. [PubMed: 21295090]
11. Stetler-Stevenson WG. Dynamics of matrix turnover during pathologic remodeling of the extracellular matrix. Am J Pathol. 1996; 148(5):1345–50. [PubMed: 8623905]
12. Kurata K, Maruyama S, Kato S, Sato W, Yamamoto J, Ozaki T, Nitta A, Nabeshima T, Morita Y, Mizuno M, Ito Y, Yuzawa Y, Matsuo S. Tissue-type plasminogen activator deficiency attenuates peritoneal fibrosis in mice. Am J Physiol Renal Physiol. 2009; 297(6):F1510–7. [PubMed: 19934446]
13. Hirahara I, Ogawa Y, Kusano E, Asano Y. Activation of matrix metalloproteinase-2 causes peritoneal injury during peritoneal dialysis in rats. Nephrol Dial Transplant. 2004; 19(7):1732–41. [PubMed: 15128883]

14. Masunaga Y, Hirahara I, Shimano Y, Kurosu M, Iimura O, Miyata Y, Amemiya M, Homma S, Kusano E, Asano Y. A case of encapsulating peritoneal sclerosis at the clinical early stage with high concentration of matrix metalloproteinase-2 in peritoneal effluent. Clin Exp Nephrol. 2005; 9(1):85–9. [PubMed: 15830280]
15. Oggionni T, Morbini P, Inghilleri S, Palladini G, Tozzi R, Vitulo P, Fenoglio C, Perlini S, Pozzi E. Time course of matrix metalloproteases and tissue inhibitors in bleomycin-induced pulmonary fibrosis. Eur J Histochem. 2006; 50(4):317–25. [PubMed: 17213041]
16. Corbel M, Belleguic C, Boichot E, Lagente V. Involvement of gelatinases (MMP-2 and MMP-9) in the development of airway inflammation and pulmonary fibrosis. Cell Biol Toxicol. 2002; 18(1): 51–61. [PubMed: 11991086]
17. Corbel M, Caulet-Maugendre S, Germain N, Molet S, Lagente V, Boichot E. Inhibition of bleomycin-induced pulmonary fibrosis in mice by the matrix metalloproteinase inhibitor batimastat. J Pathol. 2001; 193(4):538–45. [PubMed: 11276015]
18. Tan RJ, Fattman CL, Niehouse LM, Tobolewski JM, Hanford LE, Li Q, Monzon FA, Parks WC, Oury TD. Matrix metalloproteinases promote inflammation and fibrosis in asbestos-induced lung injury in mice. Am J Respir Cell Mol Biol. 2006; 35(3):289–97. [PubMed: 16574944]
19. Aso Y, Yoneda K, Kikkawa Y. Morphologic and biochemical study of pulmonary changes induced by bleomycin in mice. Lab Invest. 1976; 35(6):558–68. [PubMed: 62893]
20. Hattori N, Degen JL, Sisson TH, Liu H, Moore BB, Pandrangi RG, Simon RH, Drew AF. Bleomycin-induced pulmonary fibrosis in fibrinogen-null mice. J Clin Invest. 2000; 106(11): 1341–50. [PubMed: 11104787]
21. Zhu L, Huang X, Choi KY, Ma Y, Zhang F, Liu G, Lee S, Chen X. Real-time monitoring of caspase cascade activation in living cells. J Control Release. 2012; 163(1):55–62. [PubMed: 22664474]
22. Zhang XX, Eden HS, Chen X. Peptides in cancer nanomedicine: drug carriers, targeting ligands and protease substrates. J Control Release. 2012; 159(1):2–13. [PubMed: 22056916]
23. Cha EJ, Jang ES, Sun IC, Lee IJ, Ko JH, Kim YI, Kwon IC, Kim K, Ahn CH. Development of MRI/NIRF 'activatable' multimodal imaging probe based on iron oxide nanoparticles. J Control Release. 2011; 155(2):152–8. [PubMed: 21801769]
24. Habibollahi P, Figueiredo JL, Heidari P, Dulak AM, Imamura Y, Bass AJ, Ogino S, Chan AT, Mahmood U. Optical imaging with a cathepsin B activated probe for the enhanced detection of esophageal adenocarcinoma by dual channel fluorescent upper GI endoscopy. Theranostics. 2012; 2(2):227–34. [PubMed: 22400064]
25. Choi KY, Swierczewska M, Lee S, Chen X. Protease-activated drug development. Theranostics. 2012; 2(2):156–78. [PubMed: 22400063]
26. Jang B, Choi Y. Photosensitizer-conjugated gold nanorods for enzyme-activatable fluorescence imaging and photodynamic therapy. Theranostics. 2012; 2(2):190–7. [PubMed: 22375157]
27. Melancon MP, Zhou M, Li C. Cancer theranostics with near-infrared light-activatable multimodal nanoparticles. Acc Chem Res. 2011; 44(10):947–56. [PubMed: 21848277]
28. Zhu L, Xie J, Swierczewska M, Zhang F, Quan Q, Ma Y, Fang X, Kim K, Lee S, Chen X. Real-time video imaging of protease expression in vivo. Theranostics. 2011; 1:18–27. [PubMed: 21461134]
29. Kurotani R, Okumura S, Matsubara T, Yokoyama U, Buckley JR, Tomita T, Kezuka K, Nagano T, Esposito D, Taylor TE, Gillette WK, Ishikawa Y, Abe H, Ward JM, Kimura S. Secretoglobin 3A2 suppresses bleomycin-induced pulmonary fibrosis by transforming growth factor beta signaling down-regulation. J Biol Chem. 2011; 286(22):19682–92. [PubMed: 21478551]
30. Moeller A, Ask K, Warburton D, Gauldie J, Kolb M. The bleomycin animal model: a useful tool to investigate treatment options for idiopathic pulmonary fibrosis? Int J Biochem Cell Biol. 2008; 40(3):362–82. [PubMed: 17936056]
31. Izbicki G, Segel MJ, Christensen TG, Conner MW, Breuer R. Time course of bleomycin-induced lung fibrosis. Int J Exp Pathol. 2002; 83(3):111–9. [PubMed: 12383190]
32. Kurotani R, Tomita T, Yang Q, Carlson BA, Chen C, Kimura S. Role of secretoglobin 3A2 in lung development. Am J Respir Crit Care Med. 2008; 178(4):389–98. [PubMed: 18535256]

33. Chiba Y, Kurotani R, Kusakabe T, Miura T, Link BW, Misawa M, Kimura S. Uteroglobin-related protein 1 expression suppresses allergic airway inflammation in mice. Am J Respir Crit Care Med. 2006; 173(9):958–64. [PubMed: 16456148]
34. Lynch DA, Newell JD, Logan PM, King TE Jr, Muller NL. Can CT distinguish hypersensitivity pneumonitis from idiopathic pulmonary fibrosis? AJR Am J Roentgenol. 1995; 165(4):807–11. [PubMed: 7676971]
35. Win T, Lambrou T, Hutton BF, Kayani I, Screaton NJ, Porter JC, Maher TM, Endozo R, Shortman RI, Lukey P, Groves AM. (18)F-Fluorodeoxyglucose positron emission tomography pulmonary imaging in idiopathic pulmonary fibrosis is reproducible: implications for future clinical trials. Eur J Nucl Med Mol Imaging. 2012; 39(3):521–8. [PubMed: 22258710]
36. Marsboom G, Wietholt C, Haney CR, Toth PT, Ryan JJ, Morrow E, Thenappan T, Bache-Wiig P, Piao L, Paul J, Chen CT, Archer SL. Lung ^{18}F-fluorodeoxyglucose positron emission tomography for diagnosis and monitoring of pulmonary arterial hypertension. Am J Respir Crit Care Med. 2012; 185(6):670–9. [PubMed: 22246173]
37. Chen CJ, Lee BF, Yao WJ, Cheng L, Wu PS, Chu CL, Chiu NT. Dual-phase ^{18}F-FDG PET in the diagnosis of pulmonary nodules with an initial standard uptake value less than 2. 5. AJR Am J Roentgenol. 2008; 191(2):475–9. [PubMed: 18647920]
38. Zhu L, Zhang F, Ma Y, Liu G, Kim K, Fang X, Lee S, Chen X. In vivo optical imaging of membrane-type matrix metalloproteinase (MT-MMP) activity. Mol Pharm. 2011; 8(6):2331–8. [PubMed: 22014151]
39. Cortez-Retamozo V, Swirski FK, Waterman P, Yuan H, Figueiredo JL, Newton AP, Upadhyay R, Vinegoni C, Kohler R, Blois J, Smith A, Nahrendorf M, Josephson L, Weissleder R, Pittet MJ. Real-time assessment of inflammation and treatment response in a mouse model of allergic airway inflammation. J Clin Invest. 2008; 118(12):4058–66. [PubMed: 19033674]
40. Cortez-Retamozo V, Swirski FK, Waterman P, Yuan H, Figueiredo JL, Newton AP, Upadhyay R, Vinegoni C, Kohler R, Blois J, Smith A, Nahrendorf M, Josephson L, Weissleder R, Pittet MJ. Real-time assessment of inflammation and treatment response in a mouse model of allergic airway inflammation. J Clin Invest. 2008; 118(12):4058–66. [PubMed: 19033674]
41. Zucker S, Cao J, Chen WT. Critical appraisal of the use of matrix metalloproteinase inhibitors in cancer treatment. Oncogene. 2000; 19(56):6642–50. [PubMed: 11426650]
42. Pavlaki M, Zucker S. Matrix metalloproteinase inhibitors (MMPIs): the beginning of phase I or the termination of phase III clinical trials. Cancer Metastasis Rev. 2003; 22(2–3):177–203. [PubMed: 12784996]
43. Vincenti MP, Brinckerhoff CE. Transcriptional regulation of collagenase (MMP-1, MMP-13) genes in arthritis: integration of complex signaling pathways for the recruitment of gene-specific transcription factors. Arthritis Res. 2002; 4(3):157–64. [PubMed: 12010565]
44. Baeten J, Haller J, Shih H, Ntziachristos V. In vivo investigation of breast cancer progression by use of an internal control. Neoplasia. 2009; 11(3):220–7. [PubMed: 19242603]
45. Radisky DC, Przybylo JA. Matrix metalloproteinase-induced fibrosis and malignancy in breast and lung. Proc Am Thorac Soc. 2008; 5(3):316–22. [PubMed: 18403326]

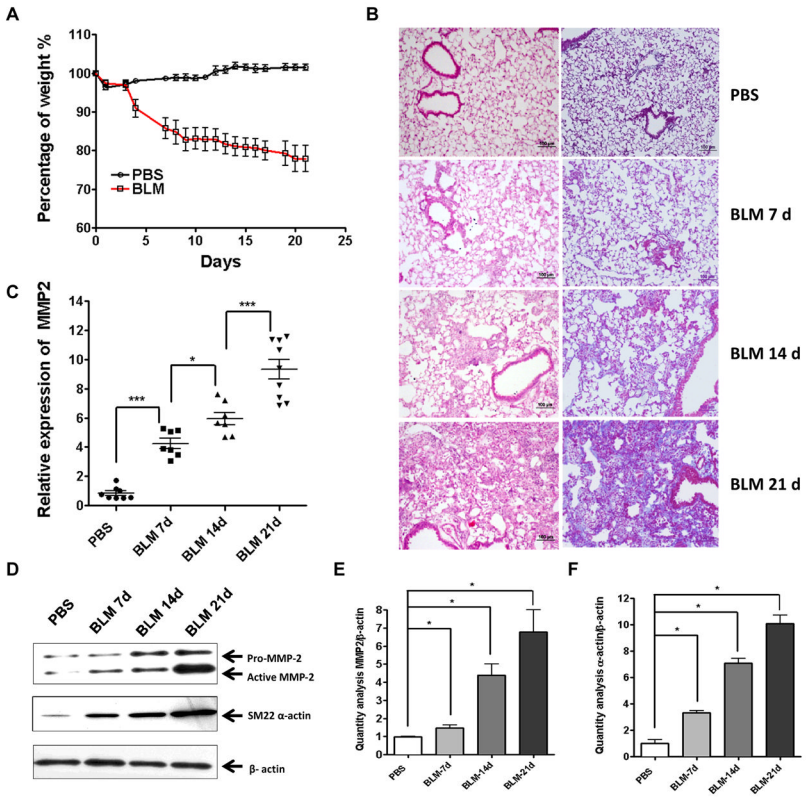

Fig. 1.

PF development and MMP2 expression. (A) Body weight curve for BLM induced-PF mice (BLM) and control group (PBS). n = 10 in each group. The average of day 0 weight was set as 100% in each group. (B) H&E staining (left) of fibrotic lung sections at 7, 14, and 21 days post-BLM administration. Masson's trichrome staining (right) to detect collagen fibers in the lung sections. Collagen was stained as blue color. Collagen expression in lungs of BLM-administered groups was found increased with the PF development, whereas very little collagen expression was found in PBS-injected group. Scale bar: 100 μm. (C) qRT-PCR quantification of *Mmp2* expression at 7, 14, and 21 day post-BLM administration. The relative expression levels of *Mmp2* mRNA were obtained by normalizing *Mmp2* mRNA levels to that of *β-actin. Mmp2* levels of PBS-treated lungs collected at 21-day were set as 1. *, $P < 0.05$, and ***, $P < 0.0005$. (D) Western blot quantification of MMP2 expression (active MMP2: 72 kDa) and the correlation with α-smooth muscle actin (SM22 α-actin) expression, which is a hallmark of PF development. Beta-actin was used as a loading control. Band intensities of MMP-2 (E) and α-actin (F) were normalized by those of β-actin and were plotted. Increase of MMP-2 and α-actin expression correlated well with the increase of *Mmp2* mRNA expression. *, $P<0.05$.

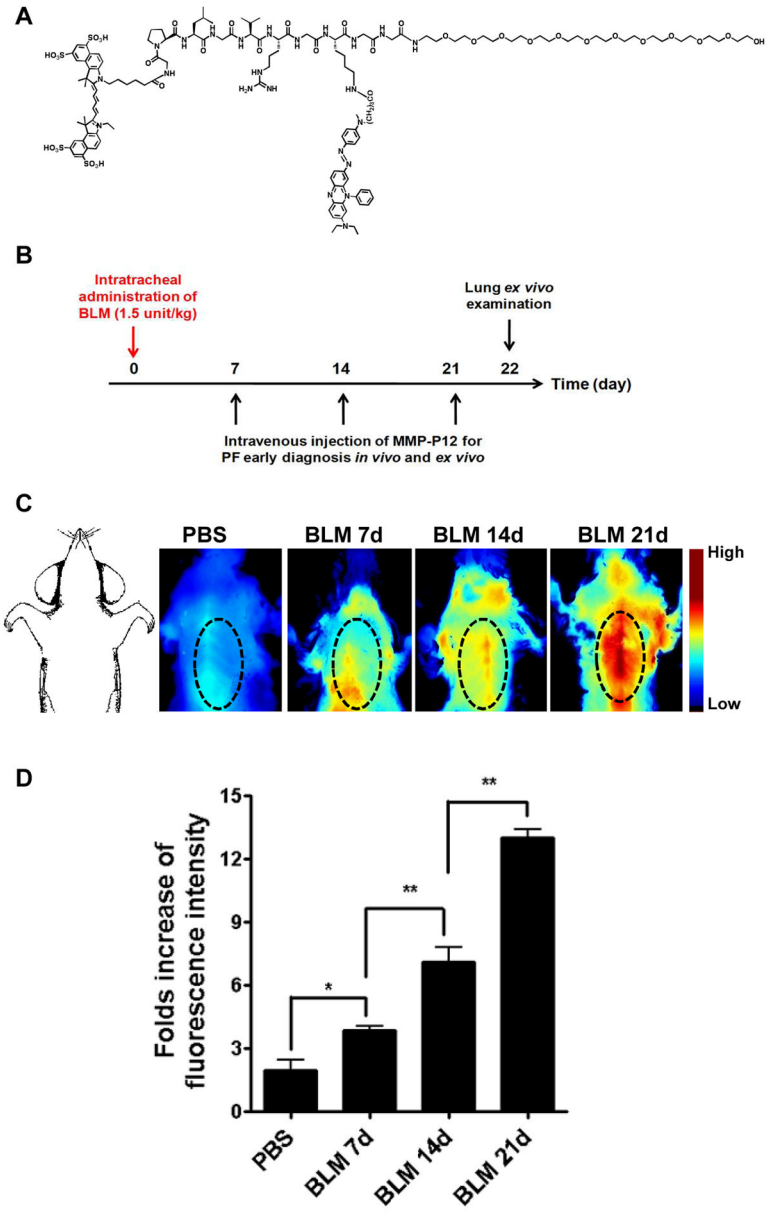

Fig. 2.

In vivo detection of PF at different stages. (A) Chemical structure of MMP-P12. (B) Experimental protocol for inducement and visualization of PF in mouse model. (C) *In vivo* imaging of lung fibrosis at different stages (7, 14 and 21 days post-BLM administration). Mice were intravenously injected with 100 nmol of MMP-P12 and 2 h later, imaged by Maestro 2.0. Fluorescence intensity became stronger as fibrosis developed. All the images were compared under the same condition. The color bar indicates radiant efficiency (low, 0; high, 0.0905×10^6). (D) Quantification of fluorescence intensity in the region of interest (ROI) shown in C (dotted circle). Compared to control group (PBS treated lungs), 3.86±0.36, 7.11±1.21, and 12.99±0.7-fold higher fluorescence signals were obtained at 7, 14, and 21 day post-BLM lungs. n = 5. *, $P < 0.05$, **, $P < 0.005$.

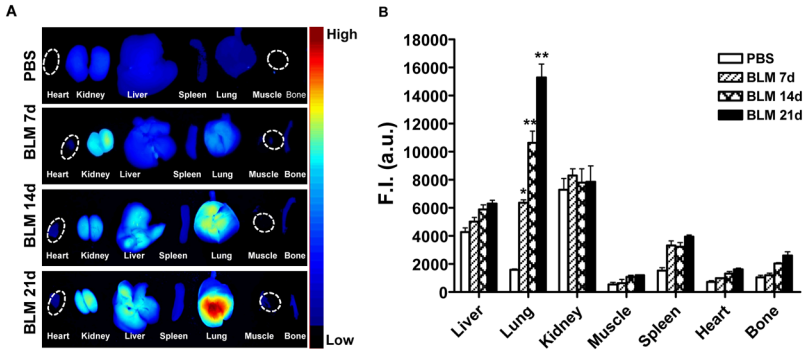

Fig. 3.

MMP-P12 activations in lung fibrosis model detected *ex vivo*. (A) Several main organs were removed from the mouse after *in vivo* imaging, which were put on a black paper for *ex vivo* analysis. Fibrosis lung at different stages showed different fluorescent signals, while the signals for the other organs remained low except kidney and liver. The color bar indicates radiant efficiency (low, 0; high, 0.147×10^6). (B) ROI of each organ (using whole tissue) was quantified at various time points as indicated and was normalized by mouse body weight. Y-axis is the fluorescence signal intensity in arbitrary unit. *, $P < 0.05$, **, $P < 0.005$.

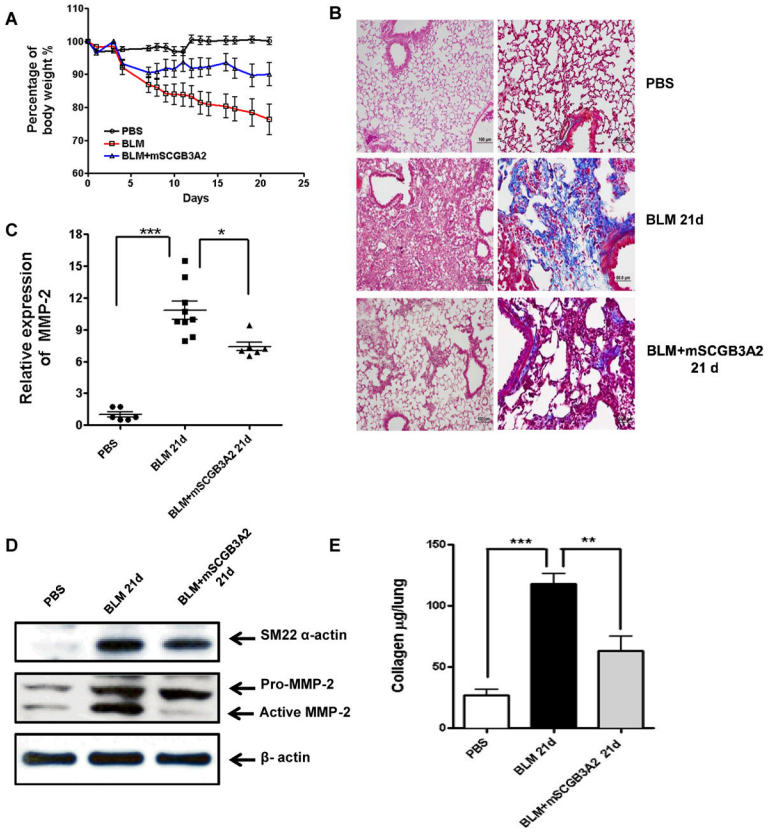

Fig. 4.

Effect of SCGB3A2 on fibrosis development and MMP2 activity in day 21 PF model with (BLM+mSCGB3A2 21d) and without (BLM 21d) mSCGB3A2 treatment. (A) Body weight curve of BLM-treated mice given SCGB3A2 (BLM+mSCGB3A2). The weight curves for PBS and BLM-treated mice are the same as those shown in Fig. 1. n = 6. (B) H&E staining (left) of fibrotic lung sections. Scale bar: 100 μm. Masson's trichrome staining to detect collagen fibers in the lung sections of day 21. Scale bar: 50 μm. Collagen was stained as blue color. An increased amount of collagen was found in 21 days PF model, while very limited collagen was found in SCGB3A2 treated lung section. (C) qRT-PCR analysis of *Mmp2* expression in day 21 PF model with (BLM+mSCGB3A2 21d) and without (BLM 21d) mSCGB3A2 treatment. The relative expression level of *Mmp2* mRNA was obtained after normalizing to *β-actin* mRNA level, and expressed using *Mmp2* levels of PBS-treated lungs as 1. *, P<0.05, and ***, P < 0.0005. (D) Western blot analysis of MMP-2 (active MMP2: 72 kDa) protein in BLM-treated lungs with (BLM+SCGB3A2) and without (B21d) mSCGB3A2 treatment. (E). Hydroxyproline content (μg/lung) of control (PBS), BLM-treated lungs with (BLM+mSCGB3A2 21d) and without (BLM 21d) mSCGB3A2 treatment, measured on day 21 of PF model. **, P<0.01, ***, P<0.001.

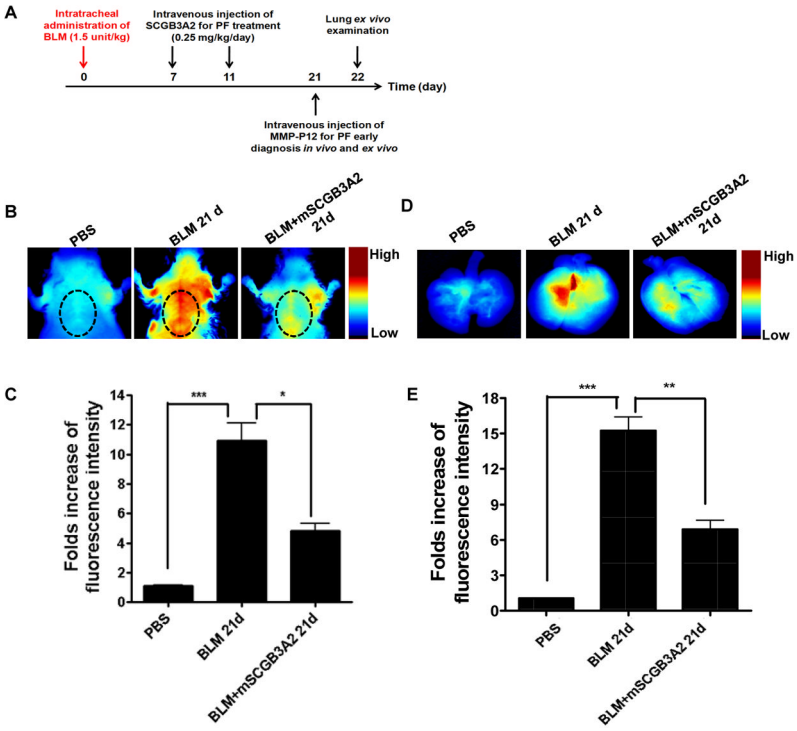

Fig. 5.

Response to SCGB3A2 treatment in PF model monitored by MMP-P12. (A) Experimental protocol for inducement, treatment and visualization of PF in mouse model. (*B*) *In vivo* imaging of lung fibrosis at 21 days in BLM mouse model and those treated with SCGB3A2 by Maestro 2.0 (optical imaging). All images were compared under the same condition. The color bar indicates radiant efficiency (low, 0; high, 0.0726×10^6). (C) Quantification of fluorescent signal from *in vivo* imaging by drawing the whole lung as ROI and was normalized by mouse body weight. Compared to control group, BLM-induced PF with SCGB3A2 treatment mice model showed a decreased fluorescent signal increment (4.82±0.87) compared with that of the PF model without treatment (10.92±2.06). (D) *Ex vivo* optical imaging of lung tissues from PBS group, BLM induced fibrotic and mSCGB3A2 treated group were compared in the same condition. The color bar indicates radiant efficiency (low, 0; high, 0.101×10^6). (E) Quantification of fluorescent signal extracted from lung section and was normalized by mouse body weight. Compared to control group, BLM-induced PF with SCGB3A2 treatment mice model showed a decreased fluorescent signal increment (6.89±1.31) compared with that of PF model without treatment (15.26±1.99). *, $P< 0.05$, **, $P < 0.005$, ***, $P < 0.0005$ (n=5).

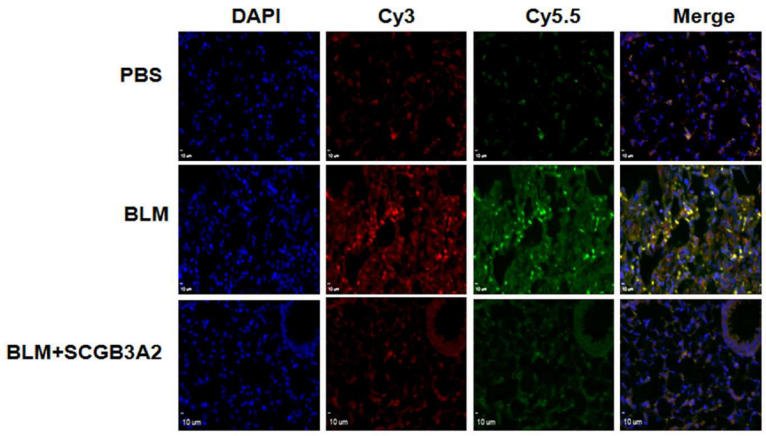

Fig. 6.

Co-localization of MMP-2 expression and cleaved MMP-P12 biodistribution in normal (PBS), fibrotic (BLM) and fibrosis recovered (BLM+SCGB3A2) lung sections. Blue (DAPI) stains nuclei, red color (Cy3) shows the expression of MMP-2, and green color (Cy5.5) shows the biodistribution of MMP-P12 in lung section. The Cy3 and Cy5.5 merged images are seen in yellow (Merge), demonstrating that a majority of red and green signals overlap. Original magnification: ×400. Scale bar: 10 μm.